ACS APPLIED MATERIALS & INTERFACES

Research Article

www.acsami.org

# Tailoring the Nanostructured Surfaces of Hydroxyapatite Bioceramics to Promote Protein Adsorption, Osteoblast Growth, and Osteogenic Differentiation

Kaili Lin,[†,‡] Lunguo Xia,[†,§] Jingbo Gan,[⊥] Zhiyuan Zhang,[§] Hong Chen,[*,⊥] Xinquan Jiang,[*,§] and Jiang Chang[*,‡]

[‡]State Key Laboratory of High Performance Ceramics and Superfine Microstructure, Shanghai Institute of Ceramics, Chinese Academy of Sciences, 1295 Dingxi Road, Shanghai 200050, China

[§]Department of Oral and Maxillofacial Surgery, College of Stomatology, Ninth People's Hospital, School of Medicine, Shanghai Jiao Tong University, Shanghai 200011, China

[⊥]College of Chemistry, Chemical Engineering and Materials Science, Soochow University, Suzhou 215123, Jiangsu, China

Supporting Information

**ABSTRACT:** To promote and understand the biological responses of the implant via nanostructured surface design is essential for the development of bioactive bone implants. However, the control of the surface topography of the bioceramics in nanoscale is a big challenge because of their brittle property. Herein, the hydroxyapatite (HAp) bioceramics with distinct nanostructured topographies were fabricated via hydrothermal treatment using $\alpha$-tricalcium phosphate ceramic as hard-template under different reaction conditions. HAp bioceramics with nanosheet, nanorod and micro-nanohybrid structured surface in macroscopical size were obtained by controlling the composition of the reaction media. Comparing with the traditional sample with flat and dense surface, the fabricated HAp bioceramics with hierarchical 3D micro-nanotextured surfaces possessed higher specific surface area, which selectively enhanced adsorption of specific proteins including Fn and Vn in plasma, and stimulated osteoblast adhesion, growth, and osteogenic differentiation. In particular, the biomimetic features of the hierarchical micro-nanohybrid surface resulted in the best ability for simultaneous enhancement of protein adsorption, osteoblast proliferation, and differentiation. The results suggest that the hierarchical micro-nanohybrid topography might be one of the critical factors to be considered in the design of functional bone grafts.

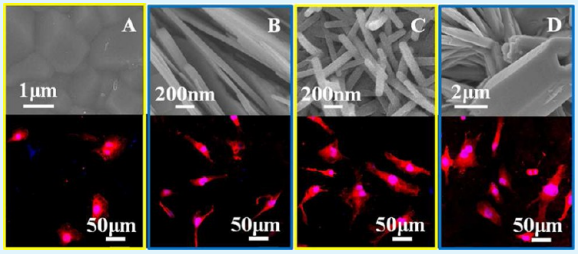


**KEYWORDS:** *surface topography, hydroxyapatite, protein adsorption, osteoblast, bone graft, osteoinduction*

## 1. INTRODUCTION

The bone graft materials usually act as a temporary matrix for cell proliferation, osteogenic differentiation, and extracellular matrix (ECM) deposition with consequent bone growth until the new bone tissue is fully formed in the defects. Therefore, the ideal materials for bone regeneration should possess excellent biocompatibility and osteoinductivity. Hydroxyapatite (HAp) bioceramic has been widely used as bone graft due to its good biocompatibility, bioactivity, high osteoconductivity, and similarity to the inorganic component of hard tissues in mammals.[1] However, it is generally considered that the traditional HAp bioceramics lack the osteoinductive ability to induce osteogenic differentiation of the stem cells and osteoblasts and to stimulate new bone formation, which is essential for regeneration of large bone defects.[2,3] Some recent studies showed that HAp/TCP composite bioceramics with specified surface microporous structure revealed osteoinductivity, which suggested that the osteoinductive potential of calcium phosphate bioceramics can be developed by controlling material characteristics such as chemical composition, surface microporous structure, and geometry, which in turn enhance bioactive protein adsorption, resorption rate and cell-material interactions.[2,3] Especially, it is suggested that, when a medical device is implanted into the human body, the initial event is the adsorption of various proteins, such as immunoglobulins, fibrinogen, vitronectin, and fibronectin, etc., from blood and other tissue fluids to the graft surface.[4] It is believed that the ability to concentrate various bone growth factors under physiological conditions should be necessary for the osteoinduction of calcium phosphate bioceramic grafts.[2] The preadsorbed proteins stimulate the recruitment of mesenchymal stem cells (MSCs) and osteoblasts, and modulate the cell adhesion, migration, proliferation, and expression of osteogenic genes.[5,6]

Received: May 31, 2013
Accepted: July 17, 2013
Published: July 17, 2013

  

The surface morphological/topographic design is considered as a potent approach to improve the bioactivity and biological responses of the grafts.[7−18] Some other studies on metal implants have shown that the surface modification with special micro/nanostructures can imitate the hierarchical features of natural bones at a certain extent to accelerate the cell adhesion,[9,10,13] migration,[7,12−14] proliferation,[9,10,15] differentiation,[8−11,16−18] and subsequently successful osseointegration of the implants.[8,11,12] Furthermore, the micro/nanostructured grafts possess higher specific surface area, which will provide much more adsorption sites to adsorb bioactive molecules.[9,10] Some in vitro studies also confirmed that the nano/microstructured surfaces could enhance the osteogenic differentiation of MSCs and osteoblasts even in the absence of growth factors,[17−19] subsequently leading to the acceleration of osseointegration and bone regeneration.[20] Therefore, improved bone defect healing may be achieved through tailoring the surface structures of bone grafts.[8,11,12,21,22]

However, few studies on controllable fabrication and biological responses of HAp bioceramics with micro-nanostructured topographies have been reported so far, because the controllable creation of surface topographies for bulk ceramic materials such as HAp bioceramics in macroscopical size is still a great challenge because of their brittleness. Most of the work up to now was only focused on the control of the crystal size and micropore size by modulation of the sintering process,[2,6,20,23] or introduction of the surface roughness in microscale level via polishing treatment.[24] The biological behavior of bone forming cells on micro-nanostructured topographies of HAp is still not well understood. Therefore, it is of great importance to achieve the control of micro- to nanotopography of bioceramics, and to illustrate its effects on osteogenic differentiation of osteoblasts, which is critical for designing optimal biomaterials for bone regeneration applications.

Recently, we have found that the morphologies of HAp particles could be well controlled using hard-templates as precursors,[25] which indicated a possible way to obtain controllable micro/nanotopographic surfaces on calcium phosphate bioceramics. In this work, fabrication of HAp bioceramics with nanostructured surface topographies using $\alpha$-tricalcium phosphate [$\alpha$-$Ca_3(PO_4)_2$, $\alpha$-TCP] ceramics as precursors under hydrothermal reaction conditions was investigated, and the effect of the reaction media on the morphologies of the obtained surface structures was evaluated. Our hypothesis is that the fabricated HAp bioceramics with nanostructured surface topographies may promote the early biological responses at the cell-HAp bioceramic interface via enhancing the adsorption of proteins, stimulating cell adhesion and differentiation, and ultimately promoting bone regeneration. Therefore, the effect of the HAp bioceramic with nanostructured surface topographies on protein adsorption, MC3T3-E1 osteoblast growth, and osseogenic differentiation for bone tissue regeneration applications was investigated to identify the optimal surface topography.

## 2. MATERIALS AND METHODS

**2.1. Fabrication and Characterization of HAp Bioceramics with Nanosheet, Nanorod, and Micro-nanohybrid Surfaces.** The HAp bioceramics with nanosheet, nanorod, and micro-nanohybrid surfaces were fabricated via hydrothermal treatment of $\alpha$-TCP ceramic in 0.2 M $NaH_2PO_4$, 0.2 M $Na_3PO_4$, and 0.2 M $CaCl_2$ aqueous solution, respectively without using any structure-directing reagents and organic solvents. The analytical grade reagents (Shanghai Chemical Co.,Ltd., China) without further purification were used in this study. First, the $\alpha$-TCP powders were synthesized by chemical precipitation method. Briefly, 1000 mL of a 0.4 mol $(NH_4)_2HPO_4$ solution with a pH about 8 was vigorously stirred at room temperature, and 1000 mL of 0.6 mol $Ca(NO_3)_2$ with a pH 8 was added dropwise to produce a white precipitate. The pH of the solution was maintained at about 8 with the addition of ammonia solution throughout the mixing process. The white precipitate was then stirred for 24 h followed by washing with distilled water for 3 times. After washing, the remaining liquid was removed by vacuum filtration, and the precipitate was dried at 120 °C for 24 h. $\alpha$-TCP powders were obtained by calcining the precipitate at 1450 °C for 5 h with a heating rate of 5 °C/min. Then, the 6 wt % polyvinyl alcohol solution was added into the obtained $\alpha$-TCP powders as binder, and the powders were uniaxially pressed into pellets with a diameter of 10 mm and a thickness of 2.2 mm under a pressure of 8 MPa in a stainless steel die. Subsequently, the $\alpha$-TCP ceramic disks with diameter of 9.45 mm were obtained by sintering the green disks at 1500 °C for 5 h at a firing rate of 2 °C/min and then cooled to room temperature in the furnace. The HAp samples with different nanostructured surfaces in macroscopical size were fabricated after hydrothermal treatment of the $\alpha$-TCP ceramic disks in 0.2 M $NaH_2PO_4$, 0.2 M $Na_3PO_4$, and 0.2 M $CaCl_2$ aqueous solution, respectively, at 180 °C for 24 h. The samples obtained by reaction in 0.2 M $NaH_2PO_4$, 0.2 M $Na_3PO_4$ or 0.2 M $CaCl_2$ aqueous solution are denoted as S1, S2, and S3, respectively. After hydrothermal treatment, the samples were washed by soaking in distilled water for several times. The traditional HAp bioceramic discs with flat and dense surface (denoted as S0) were fabricated as the control sample. First, the chemical precipitated HAp nanopowders were synthesized and then calcined at 800 °C for 2 h as raw materials.[26] Because of the significantly larger shrinkage of the HAp nanopowders after sintering, the HAp nanopowders were uniaxially pressed into pellets with a bigger diameter of 12 mm as compared to that for $\alpha$-TCP ceramic disks and a thickness of about 2 mm under a pressure of 8 MPa. Subsequently, the HAp bioceramics with diameter of 9.64 mm were obtained by sintering the green disks at 1150 °C for 3 h at a firing rate of 2 °C/min and then cooled to room temperature in the furnace. The surface morphology of the samples was observed by scanning electron microscopy (SEM: JSM-6700F, JEOL, Japan). The phase of the bulk samples was characterized by X-ray diffraction (XRD, Geigerflex, Rigaku Co., Japan) with monochromated CuK$\alpha$ radiation. The specific surface area and nitrogen sorption isotherm for the samples with nanostructured topographies were measured on a Micrometitics Tristar 3000 system, while those for sample S0 with flat and dense surface was calculated from the 3D surface area. The surface wettability of the fabricated samples was characterized by measuring the contact angles using deionized water as medium on automatic contact angle meter (Kruss, Kruss GmbH Germany). Three samples from each group were analyzed and two measurements were carried out on each sample to evaluate the average contact angle. The surface energy between pure water and air (72.8 mJ $m^{-2}$) was applied to calculate the surface energy of the samples based on the Girifalco−Good−Fowkes−Young rule.[27,28]

**2.2. Study of the Protein Adsorption on HAp Bioceramics.** The fibrinogen (Fg), fibronectin (Fn), human

serum albumin (HSA), and vitronectin (Vn) were purchased from Cal-BioChem, Sigma and Amresco, respectively. The $Na^{125}I$ was bought from Chengdu Gaotong Isotope Corporation (China Nuclear Group). Sodium dodecyl sulfate (SDS, Sigma) and Milli-Q water (18 MΩ $cm^{-1}$, Milli-Q Biocel, Millipore) were used in all experiments.

*2.2.1. Measurement of the Adsorption of Plasma Proteins on HAp Bioceramics via Protein Electrophoresis and Western Blot.* Before plasma protein adsorption, all the HAp bioceramic samples were equilibrated in phosphate buffered saline (PBS, 0.012M, pH 7.4) buffer solution for 12 h. Subsequently, the samples were incubated in human plasma at 25 °C for 3 h under static condition. After adsorption, the samples were taken out and rinsed with PBS (three times, 10 min each) to remove the loosely adherent proteins and then exposed to 2% SDS solution at 25 °C for 3 h under shaking condition to elute the adsorbed proteins. The eluates were collected and stored at 4 °C for the following experiments. SDS-polyacrylamide gel electrophoresis (SDS-PAGE) and Western-Blot were performed as described previously.[29] Briefly, the eluates were first denatured at 100 °C for 8 min and subsequently ran on 12% reduced SDS-PAGE gels to separate proteins according to molecular weight (DYCZ-24DN Electrophoresis Cell, Beijing Liuyi Instrument Factory). The proteins were then transferred from the gel onto an Immobilon PVDF membrane (Millipore, pore size: 0.45 μm). For protein electrophoresis, the PVDF membranes were directly stained by colloidal gold total protein stain (Bio-Rad Laboratories). For Western-Blot, the membranes were cut into appropriate strips and blocked with 5% nonfat dry milk. The strips were incubated with the primary antibodies at the dilution rate of 1:1000 to Fg, Fn, HSA, or Vn, and then were incubated with the appropriate alkaline phosphatase-conjugated secondary antibody with dilution rate of 1:1000. The substrate system used to develop a color reaction for alkaline phosphatase was 5-bromo-4-chloro-3-indolyl phosphate (BCIP) and nitroblue tetrazolium (NBT) supplied by Amresco. Finally, colloidal gold-stained PVDF membranes (protein electrophoresis) and immunoblotted PVDF strips (Western-Blot) were scanned by a desktop scanner to determine band molecular weights and intensities.

*2.2.2. Quantitative Analysis of Fg and HSA Adsorption on HAp Bioceramics from Human Plasma via Radiolabeling Method.* As a precise and quantitative technique, we applied the radiolabeling method to quantitatively evaluate the topographic effect of HAp bioceramics on protein adsorption,[30] and the Fg and HAS were used as the protein models. The Fg and HSA was first radiolabeled with $^{125}I$ using iodine monochloride (ICl) method, then the labeled proteins were passed through an AG 1-X4 column (Bio-Rad, dry mesh size: 100−200) to remove the unbound iodide by ion exchange.[31] To study the adsorption of Fg from plasma, the labeled Fg (Fg-I) was added to human plasma in 10% proportion to the endogenous Fg level (viewed as 3.0 mg/mL).[32] After equilibration in PBS for 12 h, the samples were placed in 96-well tissue culture plate containing 250 μL of Fg-I added plasma solution at 25 °C for 3 h. Thereafter the samples were rinsed with PBS (three times, 10 min each), wicked onto filter paper, and transferred to clean tubes for radioactivity determination using an Automatic Gamma Counter (Elmer 2480, Perkin-Elmer Life Sciences, Wallac Wizard 2TM). Each measurement was done in triplicate and radioactivity was converted to adsorbed protein amount. For the study of HSA adsorption from plasma, the labeled HSA (HSA-I) was added to human plasma in 1% proportion to the endogenous HSA level (viewed as 45.0 mg/mL), then HSA adsorption from plasma experiment was conducted in the same way as that for the analysis of Fg adsorption.

**2.3. Cell Cultures on HAp Bioceramics.** *2.3.1. Cell Culture and Seeding.* MC3T3-E1 murine preosteoblasts were cultured in the alpha-minimum essential medium (α-MEM, Gibco BRL, Grand Island, NY, USA) with 10% fetal bovine serum (Gibco BRL, Grand Island, NY, USA) and 1% penicillin/streptomycin. Cultures were maintained at 37 °C in a fully humidified atmosphere of 5% $CO_2$ in air. The culture medium was changed every 3 days. Cells were passaged with the treatment of trypsin/EDTA (0.25% w/v trypsin, 0.02% EDTA). The cells were resuspended in fresh culture medium, and then seeded on the HAp bioeramics in 24-well tissue culture plates. A seeding density of $2 \times 10^4$ cells/well was used for studies on attachment, proliferation, and osteogenic differentiation assays.

*2.3.2. Adhesion and Growth of the Seeded MC3T3-E1.* The MC3T3-E1 cells in α-MEM with 10% FCS were seeded on the HAp bioceramics and allowed to attach for 2 and 6 h. At the prescribed time points, the samples were removed from the culture medium. The amount of the nonadhesive cells in the supernatant, the nonadherent cells on the HAp bioceramic surfaces after removing by rinsing with PBS solution, and those adherents on the tissue culture plate after detaching with trypsin/EDTA was analyzed using the flow cytometer FACSCalibur (BD Biosciences, Franklin Lakes, NJ, USA). The cell adhesion amount was then calculated in percent relative to the initial seeding cell number. All experiments were done in triplicate.

*2.3.3. Morphology of the Seeded MC3T3-E1.* After culture for 2 and 6 h, the samples were taken out and rinsed with PBS to remove the nonadherent cells. The adherent cells were fixed in 4% paraformaldehyde for 30 min, and then rinsed with PBS two times. Then the samples were treated with 0.1% Triton X-100 in PBS to permeabilize the cells for 10 min and then the nonspecific binding sites were blocked with 1% BSA in PBS for 30 min. The actin cytoskeletons were labeled by incubating with Phalloidia-TRITC (Sigma) for 30 min. After rinsing with PBS, the cell nuclei was contrast-labeled in blue by 4′,6-Diamidino-2-phenylindole dihydrochloride (DAPI, Sigma), then mounted on glass slides using Fluoromount (Sigma). The confocal laser scanning microscopy (Leica, Wetzlar, Germany) was used to visualize the actin cytoskeletons of the cells. Furthermore, after culture for 1 day, the samples were fixed in 2.5% glutaraldehyde overnight at 4 °C. The samples were washed three times with PBS for 5 min, and then dehydrated by the increasing concentrations of methanol. Finally, the samples were dried by hexamethyldisilazane, sputter-coated with gold and examined by SEM (JSM-6700F, JEOL, Japan) to observe the adhesion and growth of MC3T3-E1 cells on HAp bioceramics.

*2.3.4. Cell Proliferation Assay.* For the cell proliferation assay, MC3T3-E1 cells were cultured on HAp bioceramics in 24-well tissue culture plates up to 7 days. Three pieces of cultured samples for each group were washed twice with PBS. Four hundred microliters of DMEM with supplement 40 μL of 5 mg/mL 3-(4,5-dimethylthiazol-2-yl)-2,5-diphenyl tetrazolium bromide (MTT: Amresco, Solon, OH, USA) solution was added and incubated at 37 °C for 4 h to form MTT formazan. The medium was then replaced with 400 μL of dimethyl sulfoxide (DMSO, Sigma) and vibrated for 15 min in order to

dissolve the formazan. Finally, the absorbance was measured at 490 nm by ELX Ultra Microplate Reader (BioTek, USA).

*2.3.5. Alkaline Phosphatase (ALP) Activity Assay.* The level of ALP activity was assayed by measuring the transformation of p-nitrophenyl-phosphate (pNPP: Sigma, St. Louis, USA) into p-nitrophenol (pNP) after cell culture for 4, 7, and 10 days.[33] Briefly, the cells were detached from the HAp bioceramics using trypsin/EDTA, and centrifuged for 5 min at 1000 rpm after washing twice with PBS. The cells were resuspended in lysis buffer with 0.2% pNP. ALP activity was determined by measuring absorbance at 405 nm using pNPP as the substrate. Each sample was respectively mixed with 1 mg/mL pNPP in 1 M diethanolamine buffer and incubated at 37 °C for 15 min. The reaction was stopped by the addition of 3 N NaOH to the reaction mixture. The enzyme activity was quantified by absorbance at 405 nm (BioTek, USA). The total protein content was determined with the Bradford method in aliquots of the same samples with the Bio-Rad protein assay kit (Bio-Rad, Richmond, USA), read at 630 nm and calculated according to a series of BSA (Sigma) standards. The ALP activity was expressed as absorbance at 405 nm (OD value) per milligram of total cellular proteins. All experiments were performed in triplicate.

*2.3.6. RNA Isolation and Gene Expression by Real-Time PCR Analysis.* Total cell RNA was isolated from cells cultured on HAp bioceramics at day 4 and 7. At each time point, the cells were detached and centrifuged at 1000 rpm for 5 min after washing twice with PBS, then the cells were resuspended in Trizol reagent (Invitrogen, Carlsbad, USA). The cDNA was synthesized using a Prime-Script RT reagent kit (Takara Bio, Shiga, Japan) according to manufacturer's recommendation. Highly purified gene-specific primers for type I collagen (Col I), bone sialoprotein (BSP), osteocalcin (OCN), osteopontin (OPN) and the housekeeping gene, GAPDH as shown in Table S1 (see the Supporting Information), were synthesized commercially (Shengong, Co. Ltd. Shanghai, China). Quantification of all cDNA of bone marker genes was performed with Bio-Rad My$^{iQ}$ single color Real-time PCR system. All experiments were done in triplicate to obtain the average Data.

**Statistical Analysis.** The means and standard deviations of data were calculated. Differences between groups were analyzed by one-way analysis of variance. The statistical analysis was conducted using SAS 9.0 (SAS Institute, Cary, NC, USA). The difference was considered statistically significant when $p$ value is less than 0.05.

## 3. RESULTS

**3.1. Characterization of HAp Bioceramics.** The topographic surface images of the fabricated samples S1∼S3 and control sample S0 are presented in Figure 1. The results clearly revealed that the topographic surfaces of HAp bioceramics could be facilely regulated via hydrothermal treatment of the $\alpha$-TCP ceramic precursor in different reaction media. Sample S1, which was obtained by transformation of $\alpha$-TCP ceramic precursor in $NaH_2PO_4$ solution, consisted of a smooth surface and ultralong sheetlike shape (nanosheet) with thickness of about 100 nm, widths 2−10 $\mu$m, and lengths up to hundreds of micrometers, and almost no particles or rods were detected. In contrast, when the $Na_3PO_4$ solution was used, the obtained HAp bioceramics were consisted of nanorods with diameters of about 100 nm and lengths up to 8 $\mu$m (sample S2). Sample S3 illuminated that the topographic surface after hydrothermal treatment of the $\alpha$-TCP ceramic precursor in $CaCl_2$ solution

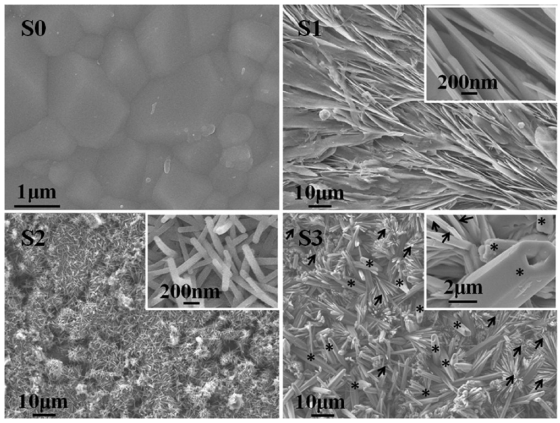


**Figure 1.** FESEM images of the control sample S0 and the fabricated HAp bioceramics with differently topographic surfaces: nanosheet (S1), nanorod (S2), and micro-nanohybrid (S3).

was constructed by the hybrid of nanorods (indicated by ↓) and microrods (indicated by *). The diameter of the nanorods and microrods is about 80−120 nm and 1−4 $\mu$m, respectively. The length of them reached about 10−20 $\mu$m. As expected, control sample S0 showed the fully flat and dense surface with an average grain size about 0.9 $\mu$m.

Figure 2 shows the XRD patterns of nanosheet (S1), nanorod (S2), and micro-nanohybrid (S3) samples after

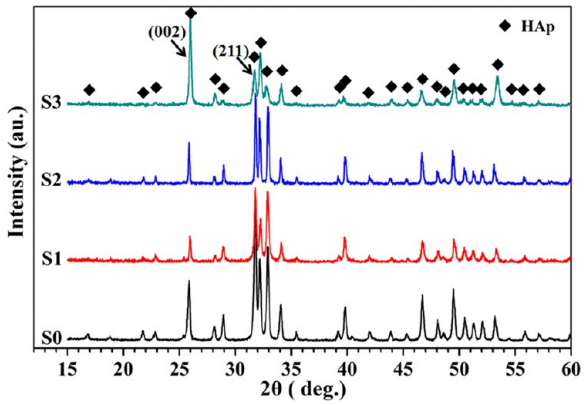


**Figure 2.** XRD patterns of the control sample (S0) and the samples with differently topographic surfaces: nanosheet (S1), nanorod (S2), and micro-nanohybrid (S3).

hydrothermal treatment of the $\alpha$-TCP ceramics in different solutions and the control sample (S0). All diffraction peaks of the samples S0−S3 could be identified as HAp (JCPDS card: No. 74−0566). Thus, the $\alpha$-TCP precursors were completely converted to HAp after hydrothermal treatment at 180 °C for 24 h in different solutions. None intermediate compounds, such as $CaHPO_4 \cdot 2H_2O$ (DCPD) and $Ca_8(HPO_4)_2(PO_4)_4 \cdot 5H_2O$ (OCP) were observed. The shape of the sharp diffraction peaks indicated that the fabricated HAp bioceramics were fairly well-crystallized, which was attributed to the hydrothermal reaction in the fabrication process. The sharp and intensive (002) peak in sample S3 indicated that the hydroxyapatite crystals preferred to be aligned apparently along the $c$-axis of HAp.[34,35] Furthermore, the HAp crystal orientation degree of the fabricated samples S0−S3 was calculated through analysis of the ratio of the specified XRD peak intensities ($R$) according to a method reported

previously.[34,35] The $R$ value was directly proportional to the orientation degree of the HAp crystals and was decided by intensity ($I$) of diffraction peaks at $2\theta$ = 25.8° for (002) and 31.8° for (211). The calculated $R$ values for S0, S1, S2, and S3 were 0.372, 0.376, 0.292, and 2.004, respectively, which further confirmed that the orientation of S3 was apparently higher than that of the other samples.

The results showed that the surface energy of all three nanostructured samples was higher than that of the control sample with smooth surface, and the surface energy of S3 was remarkablely higher than that of other two nanosamples, which was correlated with the highest crystal orientation degree of the S3 sample (see Table S2 in the Supporting Information). Moreover, porous structures with a pore size distribution between 3 and 140 nm were formed by the aggregation of the nanocrystals in the fabricated samples S1∼S3 resulting in higher specific surface area ($S_{BET}$) as compared with sample S0, which were confirmed by the nitrogen adsorption−desorption isotherms and the density functional theory (DFT) pore size distribution curves (Figure 3). The $S_{BET}$ values of S1, S2, and

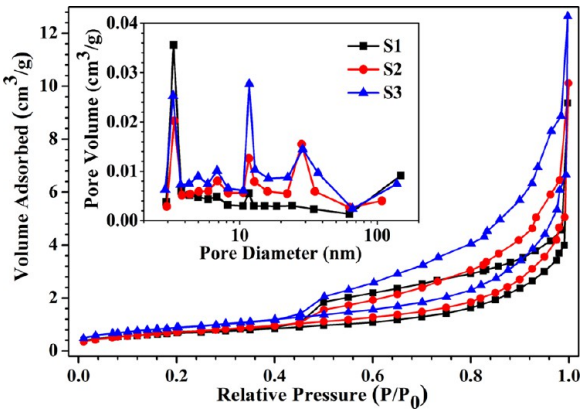


**Figure 3.** DFT pore size distribution of the fabricated HAp bioceramics with differently topographic surfaces: nanosheet (S1), nanorod (S2), and micro-nanohybrid (S3).

S3 were 2.78 ± 0.45, 2.89 ± 0.26, and 3.66 ± 0.51 $m^2/g$, respectively, whereas the calculated surface area for control sample S0 with flat and dense surface was only about 0.0006 $m^2/g$. It is interesting that the sample S3 with micro-nanohybrid structures possessed excessively higher pore volume with pore size around 12 nm. According to the International Union of Pure and Applied Chemistry, the fabricated nanostructured surfaces could be identified as a type H4 hysteresis loop deriving from particle aggregates with slit-shaped pores.[36]

**3.2. Protein Adsorption on HAp Bioceramics.** The SDS-PAGE results gave an overview of plasma protein adsorption behaviors on different samples (Figure 4a). It was obvious that the band integrated intensities on surfaces with nanomicro topographic structures were significantly stronger than that on flat and dense surface suggesting the higher protein adsorption. The Western-Blot technique was employed to further evaluate the topographic effect of HAp nanostructures on the adsorption of the specific proteins, such as Fg, Fn, HSA, and Vn in multiprotein condition (Figure 4b). The results showed that almost no adsorption of Fg and the proteins related to cell adhesions (Fn and Vn) was observed on sample S0 except for HSA. The appearance of the HSA adsorbed on S0 at 66.2 kDa was due to the ultraly high concentration (45−80 mg/mL) of HSA presented in plasma proteins when comparing with other kinds of proteins. As expected, much more bands at 116, 66.2, 45, 35, and 25 kDa with excessively stronger intensities corresponding to the proteins of Fg, Fn, HSA, or Vn could be detected on HAp bioceramic surfaces with nanotopographic structures, especially on micro−nanohybrid sample (S3).

The radiolabeling technology was further applied to quantitatively evaluate the topographic effect of HAp bioceramic nanostructures on protein adsorption using Fg and HSA as models (Figure 5). It was clear that the adsorption

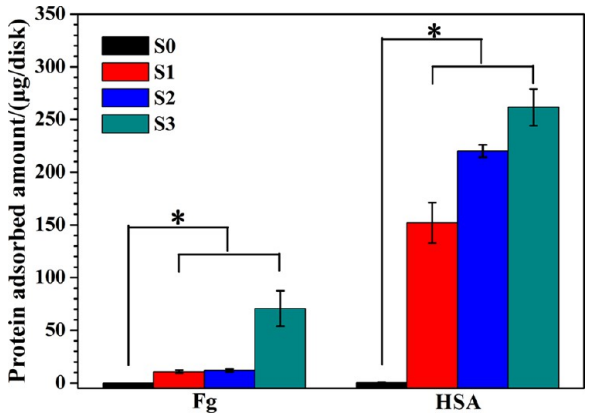


**Figure 5.** Fg and HSA adsorption on control sample (S0) and the fabricated HAp bioceramics with differently topographic surfaces: nanosheets (S1), nanorods (S2), and micro-nanohybrid (S3). *$p$ < 0.05.

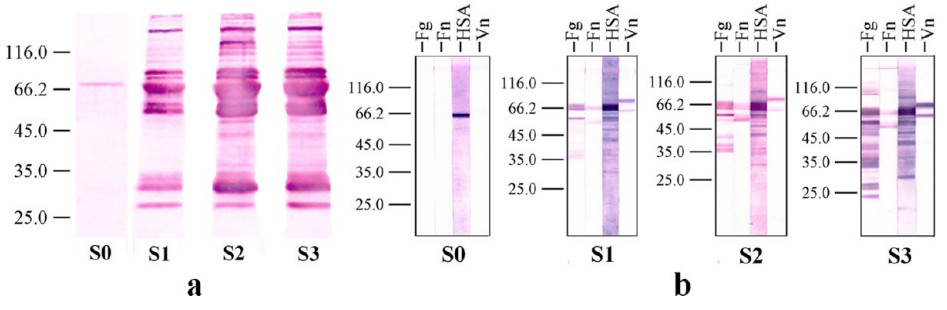


**Figure 4.** (a) SDS-PAGE and (b) Western-Blot of plasma proteins (Fg, Fn, HSA and Vn) adsorbed on samples S0−S3. The molecular weight scale is in kilodaltons (kDa).

amount of Fg and HSA on samples S1−S3 with nanostructured surfaces was remarkably higher than that on control sample with flat and dense surface (S0). Moreover, the adsorption amount of Fg and HSA was increased in the order of S1 (10.75 and 152.01 μg/disk, respectively), S2 (12.01 and 220.11 μg/disk, respectively), and S3 (70.63 and 261.57 μg/disk, respectively), which was consistent with the results of protein electrophoresis and Western-Blot data (Figure 4) and the trend of the increase in $S_{BET}$ for samples S1−S3.

**3.3. Topographic Effect of HAp Nanostructures on Osteoblast Growth.** Actin cytoskeletons were labeled to observe the early attachment of MC3T3-E1 cells after seeding for 2 and 6 h on HAp bioceramic S0−S3 (Figure 6). The cells

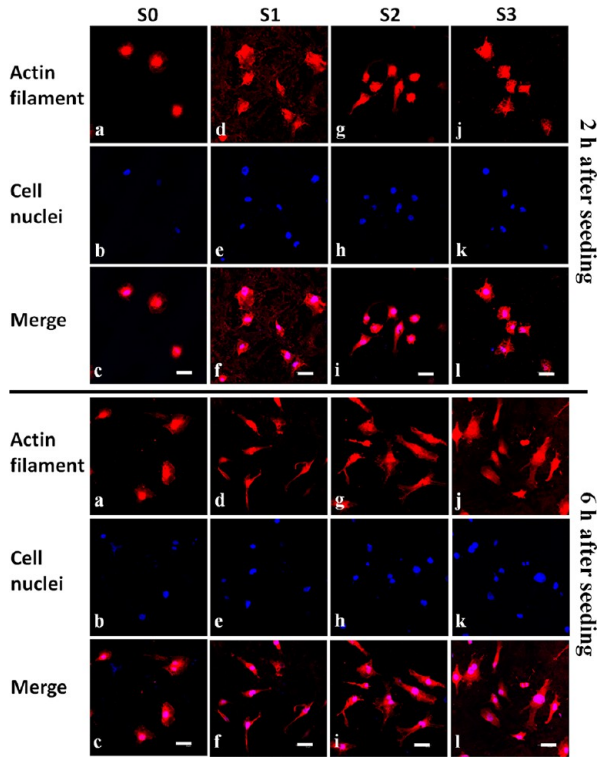


**Figure 6.** Confocal microscopic images for the topographic effect of HAp nanostructures on MC3T3-E1 cell adhesion after 2 and 6 h of seeding. Actin filament (cytoskeleton) stained red (a, d, g, j), while the cell nuclei stained blue (b, c, h, k). (c, f, i, l) represented merged images of the two fluorochromes for the samples. Scale bar= 50 μm.

attached on the HAp bioceramic with flat and dense surface (S0) showed rounded shape, almost without any filopodial after 2 h of seeding. However, the samples with topographic surfaces of nanosheet (S1), nanorod (S2), and micro-nanohybrid (S3) exhibited a significantly better early cell attachment. The MC3T3-E1 cells started to spread on the surfaces with more and apparent cytoplasmic extensions and filopodial attachments. With the increase in the seeding time to 6 h, the cells seeded on S0 spreaded slightly. On the contrary, the cells showed full adhesion with their typical fibroblastic morphology on S1−S3. More importantly, actin filaments with regular directions on samples S1−S3 with nanotopographic surfaces were well-defined by the actin microfilament system ranging parallel to the long axis of the cells. In contrast, the actin cytoskeleton formation on S0 was distributed irregularly and in short fiber concentration. Therefore, a strong directed accumulation of actin filaments on samples S1−S3 could be observed, which reflected the importance of surface topography on osteoblast growth. The phenomenon was more obvious on S3 with micro-nanohybrid structure.

The fluorescence images stained by DAPI in Figure 7A showed that the initially adherent cell number on samples S1−S3 was visually higher than that on sample S0 after seeding for 6 h. The quantitative evaluation further revealed a significant increase of adherent cells on samples S1−S3 in comparing with the control sample S0 (Figure 7B). The MTT assay was performed to compare cell proliferation of MC3T3-E1 cultured on S0−S3 samples. As shown in Figure 7C, the proliferation of MC3T3-E1 proceeded more significantly on sample S3 with micro-nanohybrid topographic surface than that on other samples.

The SEM observation was further applied to examine the topographic effect of HAp nanostructures on cell adhesion and morphology (Figure 8). Cells attached and grew well on all ceramic surfaces at day 1, while the cells on the samples with nanostructured surfaces (S1−S3) appeared much flater and spreading out better comparing with those on sample S0. In addition, much more and longer filopodials attached on the samples with nanotopographic surfaces.

*Topographic Effect of HAp Nanostructures on ALP Activity of MC3T3-E1.* Figure 9 shows the topographic effect of HAp nanostructures on ALP activity of MC3T3-E1. The ALP activity of cells cultured on all HAp bioceramics increased apparently over time throughout the assay period. However, the ALP activity of the MC3T3-E1 seeded on S2 and S3 was significantly higher than that on S0 at day 7. With the increase of the culture time to day 10, the ALP activity of the cells cultured on all samples S1∼S3 was significantly higher than that on sample S0.

*Topographic Effect of HAp Nanostructures on Osteogenic Gene Expression of MC3T3-E1.* The expression levels of osteogenesis related genes including Col I, BSP, OCN and OPN were assayed by real-time PCR after culture of MC3T3-E1 on samples S0∼S3 for 4 and 7 days (Figure 10). At day 4, the cells cultured on S2 and S3 showed increased expression of Col I, whereas the expression of OCN was increased on S1−S3, and the expression of OPN was enhanced only for cells cultured on S1 and S3. The expression of BSP was enhanced only for cells cultured on S3. Prolonging the culture time to day 7, the sample S3 with micro-nanohybrid structured surface still displayed significantly high-level expression of Col I, BSP, OCN and OPN, as compared with those on sample S0 with flat and dense surface, whereas the cells cultured on S2 only showed the enhanced expression of OPN compared with control group, and cells on S1 did not show any difference as compared with S0.

## 4. DISCUSSION

The material with initiative stimulation capacity in tissue regeneration is the major characteristic for the next generation biomaterials. Recent in vitro and in vivo studies have confirmed the biological sensitivity to the level of micro/nanostructured surfaces of the implant biomaterials.[7−18,22,37−39] For example, the titania ($TiO_2$) nanotubes and nodulars fabricated via anodization and acid-etching methods on titanium (Ti) foils strongly enhanced cellular activity as compared with a flat surface,[8−12] while ZnO nanoflowers enhances osteoblast differentiation and osteogenesis.[22] Other studies showed that the silicon (Si) nanopillars/wires obtained by laser pulse fluence or ion-etching technologies improve the cell adhesion

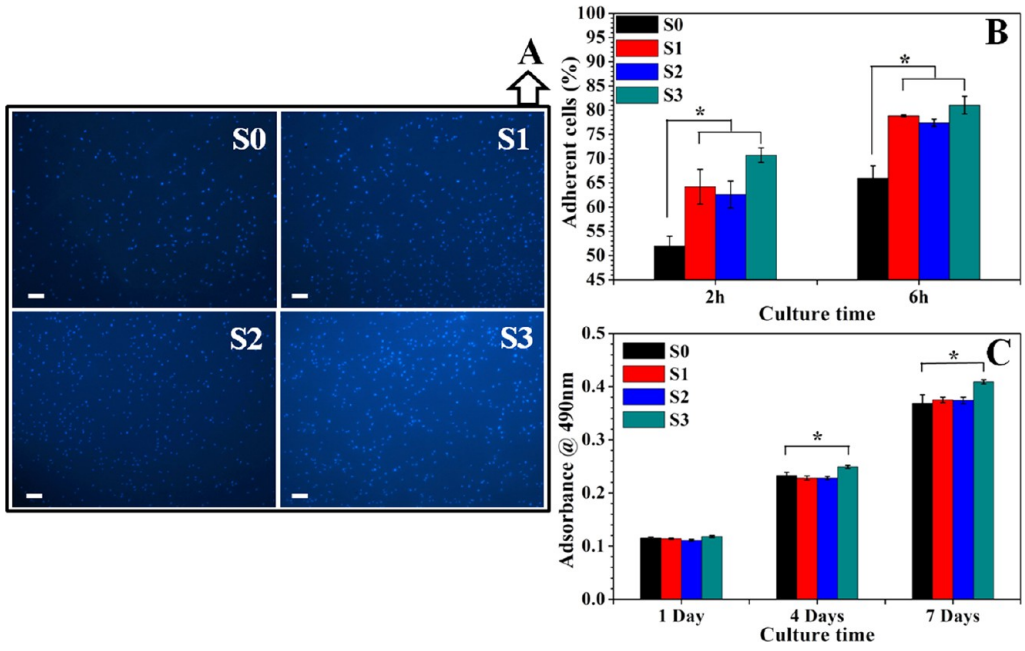


**Figure 7.** (A) Fluorescence images of the attached MC3T3-E1 cells after seeding for 6 h and stained with DAPI, (B) cell adherent percent after seeding for 2 and 6 h on samples S0−S3, and (C) MTT assay of MC3T3-E1 seeded on samples S0−S3 from 1 to 7 days for cell viability and proliferation. Scale bar = 200 $\mu$m. *$p$ < 0.05.

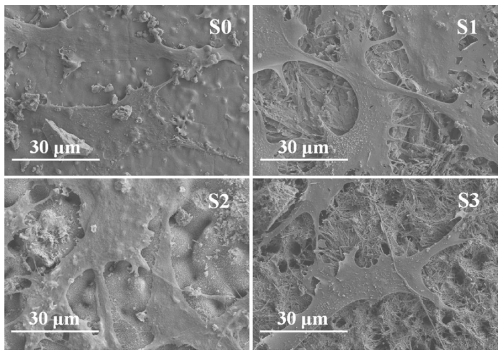


**Figure 8.** SEM observation of cell adhesion on the control sample with flat and dense surface (S0) and the samples with differently topographic surfaces of nanosheets (S1), nanorods (S2), and micro-nanohybrid (S3) after seeding for 1 day.

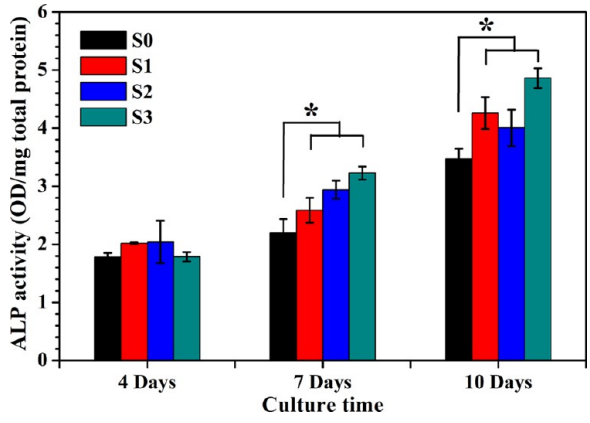


**Figure 9.** ALP activity of MC3T3-E1 cultured on control sample with flat and dense surface (S0) and the samples with different topographic surfaces of nanosheets (S1), nanorods (S2), and micro-nanohybrid (S3) after seeding for 4, 7, and 10 days. *$p$ < 0.05.

and growth,[37,38] and the patterned pits/grooves/griddings of polymer films by UV and electron beam lithography approaches stimulate osteogenic differentiation of MSCs and osteoblasts.[17,18,39] Up to now, the controllable creation of nanotopographic features on bioceramic materials such as HAp in macroscopical size is still a great challenge due to their brittleness. The biological behavior on micro/nanostructured topography of HAp is still not well understood, and the type of surface topographies, such as micro-, nano-, and/or hierarchical hybrid micro/nanoscale, which may be able to stimulate osteogenic differentiation, should be clarified for optimizaton of biomaterial design. In this study, based on our previous observation on morphology control of HAp particles using hard-template as precursors,[25] the HAp bioceramic discs with nanosheet (S1, thickness of ∼100 nm), nanorod (S2, diameters of ∼100 nm), and micro-nanohybrid (S3, mixed by nanorods in 80−120 nm and microrods in 1−4 $\mu$m) surfaces were first successfully fabricated via hydrothermal treatment of $\alpha$-TCP ceramics in $NaH_2PO_4$, $Na_3PO_4$, and $CaCl_2$ aqueous solution, respectively (Figure 1B−D).

Under hydrothermal treatment, the surface erosion occurred on $\alpha$-TCP ceramic substrates in aqueous solution, accompanying with the release of the $Ca^{2+}$ and $PO_4^{3-}$ ions into the solutions. With the increase of the ion release, the $Ca^{2+}$ and $PO_4^{3-}$ concentration in the reaction solution reached oversaturation and the HAp nucleated on the eroded substrate surfaces.[25] During this process, the substrate itself played both the roles of $Ca^{2+}$ and $PO_4^{3-}$ ion sources and the HAp crystal nucleation surface.[25] The model of $Ca_9(PO_4)_6$ clusters (Posner Clusters) with positive charge could be applied to illuminate the effect of the hydrothermal conditions on HAp morphology development. The $Ca_9(PO_4)_6$ clusters are considered as the growth unit of HAp crystals.[40] It is well-known that hexagonal HAp crystal has two types of crystal surfaces with different charges, positive on $a$ and $b$ surfaces and negative on $c$ surface.[41] Usually, hexagonal HAp crystals which grow along

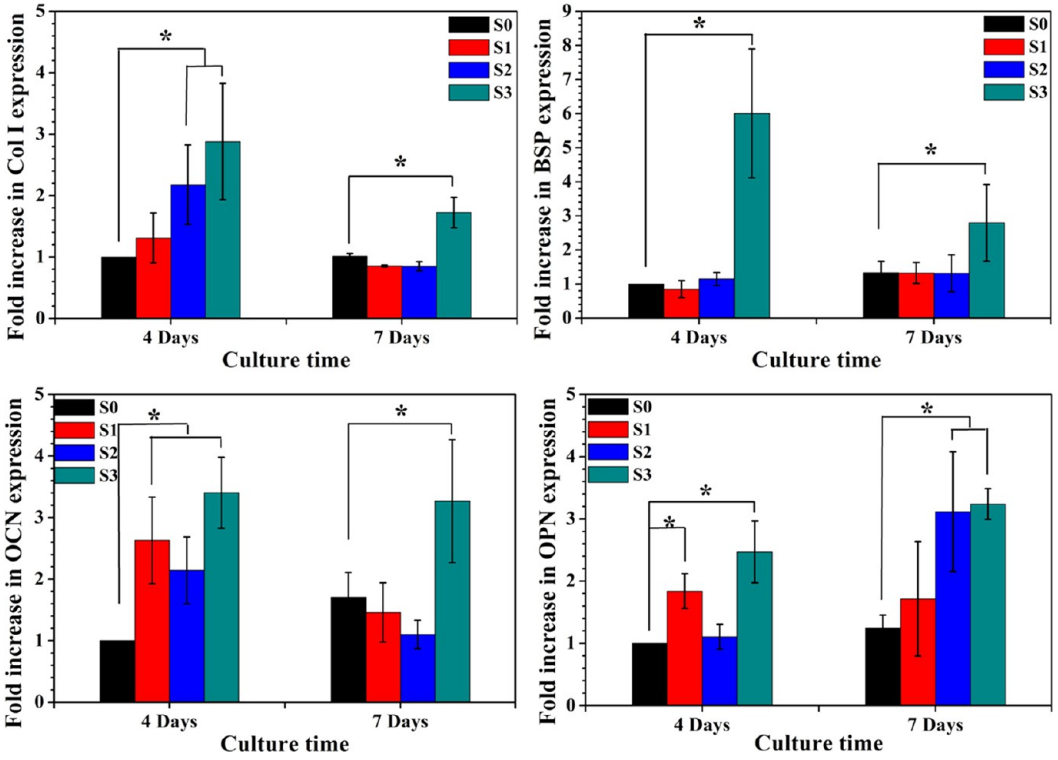


**Figure 10.** Osteogenic gene expression of MC3T3-E1 cultured on control sample with flat and dense surface (S0) and the samples with different topographic surfaces of nanosheet (S1), nanorod (S2), and micro-nanohybrid (S3). *$p < 0.05$.

the *c* axis are easily obtained because of a strong bond site for $Ca_9(PO_4)_6$ cluster in the *c*-surface direction.[42,43] In $NaH_2PO_4$ solution, the hydrolyzation of $NaH_2PO_4$ salts was greater than ionization. The major ions in the solution were $H_2PO_4^-$ and $HPO_4^{2-}$ ions. In addition, most of the $PO_4^{3-}$ ions released from the $\alpha$-TCP substrate would be hydrolyzed in the $NaH_2PO_4$ aqueous solution. Thus, there was only a small amount of $PO_4^{3-}$ ions presented in the reaction system, which resulted in fewer Posner clusters incorporating onto the *c*-surface, so that the growth of *c* surface was limited,[25] whereas the redundant $Ca^{2+}$ ions released from the $\alpha$-TCP substrate attached on the *c* surface with negative charge.[25] The growth of the *a*, *b* surfaces was enhanced, leading to the aggregation of *a*, *b* planes. Ultimately, the HAp nanosheet were obtained. However, in $Na_3PO_4$ solution, the excessive amount of $PO_4^{3-}$ ions came from $Na_3PO_4$ solution and released from $\alpha$-TCP substrate reacted quickly with $Ca^{2+}$ ions dissolved from $\alpha$-TCP substrate to form Posner clusters. The released $Ca^{2+}$ ions were rapidly consumed, which resulted in quite a few $Ca^{2+}$ ions remaining in the near of the surface of substrate. Posner clusters would attach to the *c* surface preferentially and the direction along the *c* axis developed quickly, resulting the HAp nanorod structure. When $CaCl_2$ aqueous solution was used, the $PO_4^{3-}$ ions released from the $\alpha$-TCP substrate would be quickly combined with $Ca^{2+}$ ions to form the Posner clusters, and then attached on the *c*-surface. The preferential crystal growth took place on the *c* surface. However, as a competitor, the large amount of redundant $Ca^{2+}$ ions would be competitively adsorbed on the *c* surface. The growth of the *a*, *b* surfaces in some HAp crystals was also enhanced, resulting in the hybrid of microrods and nanorods.

Our results show that the fabricated HAp bioceramics S1−S3 with micro/nanostructured surface features possessed 3D architectures (Figure 1B−D), higher $S_{BET}$ and porous structures (Figure 3), superior wettability and surface energy (Table S2), which resulted in enhanced and selective protein adsorption (Figures 4 and 5). In addition, the protein adsorption amount increased apparently with the increase of the $S_{BET}$ of the samples (Figure 5). It is well-known that Fn and Vn are the most important cell adhesion proteins that can bind to integrins on cell surface and stimulate cell attachment and/or cell spreading on biomaterials.[44−46] Fn is also thought to play an important role in early osteogenesis, as it is one of the first synthesized bone matrix proteins by osteoblasts during osteogenesis.[47,48] The apparent adsorption of Fn and Vn on our fabricated HAp bioceramic samples with topographic surfaces of nanosheet (S1), nanorod (S2) and micro-nano-hybrid (S3) was observed, whereas adsorption phenomenon was absent on tranditional HAp bioceramic samples (S0) with flat and dense surface (Figure 4b). Furthermore, it is interesting to find that the surface energy of the nanostructured HAp surfaces was correlated with the HAp crystal oriantation degree. All three nanostractured surface showed both higher surface energy and crystal oriantation degree as compared with that of the smooth surface. In addition, the surface energy of S3 was remarkablely higher than that of other two nanosamples, which was correlated with the highest crystal orientation degree of the S3 sample (see Table S2 in the Supporting Information). This result suggests that the surface energy of the HAp bioceramics, which is affected by the HAp crystal oriantation degree, plays an important role in the osteoinductive activity of the bioceramics. Together with surface topography, it is considered that the increase of the initial hydrophilicity and surface energy may promote the early bone healing response at the cell−biomaterial interface via increasing the adsorption of proteins including fibronectin, which enhances cell adhesion and ultimately promotes reponse of mesenchymal stem cells (MSCs) and osteoblasts on the implant surfaces.[28]

Accordingly, the cell attachment assay showed that the initially adherent MC3T3-E1 numbers on sample S1−S3 was about 2−3 times and 33−36% higher than those on control sample S0 after seeding for 2 and 6 h, respectively (Figure 7B). The adhesion to the graft surfaces is necessary for osteoblast spreading and differentiation.[8] The actin cytoskeleton staining (Figure 6) revealed that the topographic surfaces of S1−∼S3 induced more active filopodia formation than flat and dense surface of S0. Actin is well-developed, evenly distributed, and arrayed along the osteoblast spreading direction on samples S1∼S3 after 6 h of seeding, whereas the actin structure was poorly developed on sample S0. The enhancement of protein adsorption, such as Fn and Vn, on the surfaces of samples S1−S3 was considered to be able to promote integrin binding and the expression of cytoskeletal protein of actin, which resulted in the effective filopodia formation.[44−48] The SEM observation further confirmed that the MC3T3-E1 attached and spread much better on S1−S3 than those on S0, and the length of the extension was many times larger than the diameter of the cells. In addition, the network formation on samples S1−S3 surfaces was observed just after 1 day of seeding (Figure 8).

The ability of HAp bioceramic surface topography in promoting osteogenic differentiation of MC3T3-E1 was found in this study. As an early marker for osteogenic differentiation, ALP regulates organic or inorganic phosphate metabolism via hydrolyzation of phosphate esters, and acts as a plasma membrane transporter for inorganic phosphates.[33] Compared with sample S0, there was about 24, 18, and 41% increase in ALP activity level of the cells on samples S1, S2, and S3, respectively after 10 days of culture (Figure 9). Real-time PCR analysis of markers of Col I, BSP, OCN, and OPN was further performed for additional evaluation of osteogenic differentiation promoted by surface topography (Figure 10). Col I is the most important fibrillar type of collagen ECM component and serves as mineralization scaffolds and initiation sites for bone apatite deposition.[11] Col I is known to be an early osteogenic marker and necessary for bone matrix formation.[11] In our study, Col I expression was up-regulated at earlier time point (day 4) on samples S2 and S3, and maintained highest on sample S3 at day 7 as compared with S0. As a bone-specific marker for osteogenic differentiation, BSP is a mineralized, tissue-specific, and noncollagenous protein that is normally expressed only in mineralized tissues such as bone, dentin, cementum, and calcified cartilage, and at sites of new mineral formation. The binding of BSP to collagen is thought to be important for initiating bone mineralization and bone cell adhesion to the mineralized matrix.[49] The BSP expression on sample S3 was six and two times higher as compared with that on other smaples at day 4 and 7, respectively. As another bone-specific marker for osteogenic differentiation and secreted solely by osteoblasts, OCN is considered as the major noncollagenous component related to bone matrix deposition and mineralization and is regadred as a later marker of osteogenic differentiation.[33,50] Interestingly, OCN expression was remarkably up-regulated on samples S1−S3 at early stage of day 4. With the increase in the culture time to day 7, the high expression level for OCN on S3 was maintained. Finally, OPN is associated with the maturation stage of osteoblasts during attachment and matrix synthesis before mineralization, and is largely considered as an intermediate or relatively earlier marker of osteogenic differentiation.[33] In our study, the OPN expression for cells cultured on nanorod surfaces (S2) and micro-nanohybrid surfaces (S3) was almost 2.5 times as compared with that on flat and dense surface (S0) at day 7. The higher expression level of OCN and OPN suggested that the nanostructured bioceramic surface has the ability to stimulate osteogenic differentiation of osteoblastic cells and micro-nanohybrid topography surface (S3) has the highest stimulatory effect.[33,50]

It is well-known that the actin filaments and cell extension help the cells to anchor themselves to biomaterial surfaces, which improve the cell adhesion and spreading,[8] and the cell adhesion and spreading not only manifest interactons between cells and materials but also regulate cellular functions such as migration, proliferation, differentiation, and ECM production.[7,14−16,19] Our results indicated the fact that the nanostructured topography of HAp bioceramics could enhance adhesion, spreading, and osteogenic differentiation of osteoblasts by accelerating early cell responses such as cell attachment and spreading. Especially, the micro-nanohybrid topography surface (S3) induced cell adhesion, proliferation, and osteogenic differentiation more significantly. Previous studies showed that the micro-nanohybrid structured Ti, $TiO_2$, silicon, and alloy biomaterials simultaneously enhanced osteoblast proliferation and differentiation as comapred with single scale micro- or nanostructured topography, leading to promotion of the osseointegration on clinically relevant surfaces.[9,10] Indeed, in the context of a natural environment, the osteoblasts and MSCs in a bone tissue are surrounded by a 3D ECM from nano- to microscale.[37] Therefore, from the biomimetic viewpoint, a hierarchical structure composed of multiple micro- and nanoscale components bear a closer resemblance to biological matrices than those with single scale features, and that materials with multiscale organization are necessary for cell functioning and play critical and advantage roles for biomedical applications.[9,37,51] Taken together with the protein adsorption, osteoblast adhesion, proliferation, and osteogenic differentiation investigation, the hierarchical micro-nanohybrid topography reported here may enhance osteoinductive ability of HAp bioceramics via promoting bone formation directly in contact with the surface as well as in the surrounding tissue, which may provide insight to future development of new bone implant materials. However, further in vivo studies are required to confirm the possible application potential.

## 5. CONCLUSIONS

To enhance bone regeneration, it is essential to develop bioactive grafts with nano- and microstructured topographies, which may stimulate the cell response to biomaterial surfaces. In the present study, the bulk HAp bioceramics with nanosheet, nanorod, and micro-nanohybrid surface topographies were fabricated via hydrothermal treatment using $\alpha$-TCP ceramic as the precursor under different reaction conditions. The fabricated HAp bioceramics possessed hierarchical 3D micro/nanotextured surfaces, higher $S_{BET}$, and better wettabilities, which selectively enhanced adsorption of specific proteins such as Fn and Vn in plasma, whereas almost no protein adsorption was observed on the traditional HAp bioceramics with flat and dense surface. The nanostructured topography promoted osteoblast attachment, spreading, adhesion, proliferation, and osteogenic differentiation. In particular, the hierarchical micro-nanohybrid surfaces showed the best ability for promotion of protein adsorption and enhancement of cell proliferation and differentiation because of the biomimetic features of this kind of structure. The results suggest that the hierarchical micro-

nanohybrid topography might be one of the critical factors to consider in the design of new bone implant biomaterials.

## ■ ASSOCIATED CONTENT

### Supporting Information

Primer sequences used for real-time PCR were shown in Table S1. The contact angle and surface energy of the samples were shown in Table S2. This material is available free of charge via the Internet at http://pubs.acs.org/.

## ■ AUTHOR INFORMATION


### Corresponding Author

*E-mail: jchang@mail.sic.ac.cn (J.C.); chenh@suda.edu.cn (H.C.); xinquanj@yahoo.cn (X.J.). Tel./Fax: 86-21-52412804.

### Author Contributions

†Authors K.L. and L.X. contributed equally.


### Notes

The authors declare no competing financial interest.

## ■ ACKNOWLEDGMENTS

The author gratefully acknowledges the support of Natural Science Foundation of China (Grant 81171458, 81190132), Science and Technology Commission of Shanghai Municipality (Grant 12 nm0501600, 13NM1402102), the Funds of the Shanghai Institute of Ceramics, Chinese Academy of Sciences for Innovation of Science and Technology (Grant Y26ZC1110G), and the Funds of Key Laboratory of Inorganic Coating Materials, Chinese Academy of Sciences.

## ■ REFERENCES


(1) Costa, D. O.; Dixon, S. J.; Rizkalla, A. S. *ACS Appl. Mater. Interfaces* **2012**, *4*, 1490−1499.

(2) Yuan, H. P.; Fernandes, H.; Habibovic, P.; De Boer, J.; Barradas, A. M. C.; De Ruiter, A.; Walsh, W. R.; Van Blitterswijk, C. A.; De Bruijn, J. D. *Proc. Natl. Acad. Sci. U.S.A.* **2010**, *107*, 13614−13619.

(3) Hong, Y. L.; Fan, H. S.; Li, B.; Guo, B.; Liu, M.; Zhang, X. D. *Mater. Sci. Eng., R* **2010**, *70*, 225−242.

(4) Grinnell, F.; Feld, M.; Minter, D. *Cell* **1980**, *19*, 517−525.

(5) Lord, M. S.; Foss, M.; Besenbacher, F. *Nano Today* **2010**, *5*, 66−78.

(6) Li, X. M.; Van Blitterswijk, C. A.; Feng, Q. L.; Cui, F. Z.; Watari, F. *Biomaterials* **2008**, *29*, 3306−3316.

(7) Kaiser, J. P.; Reinmann, A.; Bruinink, A. *Biomaterials* **2006**, *27*, 5230−5241.

(8) Popat, K. C.; Leoni, L.; Grimes, C. A.; Desai, T. A. *Biomaterials* **2007**, *28*, 3188−3197.

(9) Zhao, L. Z.; Liu, L.; Wu, Z. F.; Zhang, Y. M.; Chu, P. K. *Biomaterials* **2012**, *33*, 2629−2641.

(10) Kant, K.; Low, S. P.; Marshal, A.; Shapter, J. G.; Losic, D. *ACS Appl. Mater. Interfaces* **2010**, *2*, 3447−3454.

(11) Wang, N.; Li, H. Y.; Lü, W. L.; Li, J. H.; Wang, J. H.; Zhang, Z. T.; Liu, Y. R. *Biomaterials* **2011**, *32*, 6900−6911.

(12) Park, J.; Bauer, S.; von der Mark, K.; Schmuki, P. *Nano Lett.* **2007**, *7*, 1686−1691.

(13) Du, K.; Gan, Z. H. *ACS Appl. Mater. Interfaces* **2012**, *4*, 4643−4650.

(14) Kim, D. H.; Seo, C. H.; Han, K.; Kwon, K. W.; Levchenko, A.; Suh, K. Y. *Adv. Funct. Mater.* **2009**, *19*, 1579−1586.

(15) Wang, N.; Li, H. Y.; Wang, J. S.; Chen, S.; Ma, Y. P.; Zhang, Z. T. *ACS Appl. Mater. Interfaces* **2012**, *4*, 4516−4523.

(16) Chang, H. Y.; Chi, J. T.; Dudoit, S.; Bondre, C.; van de Rijn, M.; Botstein, D.; Brown, P. O. *Proc. Natl. Acad. Sci. U.S.A.* **2002**, *99*, 12877−12882.

(17) Dalby, M. J.; Gadegaard, N.; Tare, R.; Andar, A.; Riehle, M. O.; Herzyk, P.; Wilkinson, C. D. W; Oreffo, R. O. C. *Nat. Mater.* **2007**, *6*, 997−1003.

(18) Unadkat, H. V.; Hulsman, M.; Cornelissen, K.; Papenburg, J.; Truckenmüller, R. K.; Carpenter, A. E.; Wessling, M.; Post, G. F.; Marcel, M. U.; Reinders, J. T. *Proc. Natl. Acad. Sci. U.S.A.* **2011**, *108*, 16565−16570.

(19) Kuo, S. W.; Lin, H. I.; Ho, J. H. C.; Shih, Y. R. V.; Chen, H. F.; Yen, T. J.; Lee, O. K. *Biomaterials* **2012**, *33*, 5013−5022.

(20) Zhu, X. D.; Fan, H. S.; Xiao, Y. M.; Li, D. X.; Zhang, H. J.; Luxbacher, T.; Zhang, X. D. *Acta Biomater.* **2009**, *5*, 1311−1318.

(21) Barradas, A. M. C; Yuan, H.; Van Blitterswijk, C. A.; Habibovic, P. *Eur. Cells Mater.* **2011**, *21*, 407−429.

(22) Park, J. K.; Kim, Y. J.; Yeom, J.; Jeon, J. H.; Yi, G. C.; Je, J. H.; Hahn, S. K. *Adv. Mater.* **2010**, *22*, 4857−4861.

(23) Webster, T. J; Ergun, C.; Doremus, R. H.; Siegel, R. W.; Bizios, R. *Biomaterials* **2000**, *21*, 1803−1810.

(24) Kokkinos, P. A.; Koutsoukos, P. G.; Deligianni, D. D. *J Mater. Sci. Mater. Med.* **2012**, *23*, 1489−1498.

(25) Liu, X. G.; Lin, K. L.; Chang, J. *CrystEngComm.* **2011**, *13*, 1959−1965.

(26) Lin, K. L.; Pan, J. Y.; Chen, Y. W.; Cheng, R. M.; Xu, X. C. *J. Hazard. Mater.* **2009**, *161*, 231−240.

(27) Good, R. J.; Giripalco, L. A. *J. Phys. Chem.* **1960**, *64*, 561−565.

(28) Park, J. W.; Kim, Y. J.; Park, C. H.; Lee, D. H.; Kod, Y. G.; Jang, J. H.; Lee, C. S. *Acta Biomater.* **2009**, *5*, 3272−3280.

(29) Cornelius, R. M.; Archambault, J. G.; Berry, L.; Chan, A. K.; Brash, J. L. *J. Biomed. Mater. Res.* **2002**, *60*, 622−632.

(30) Wagner, M. S.; Horbett, T. A.; Castner, D. G. *Biomaterials* **2003**, *24*, 1897−1908.

(31) Angeles, C. M.; Bale, W. F.; Spar, I. L. *Methods Enzymol.* **1983**, *92*, 277−292.

(32) Chen, H.; Zhang, Z.; Chen, Y.; Brook, M. A.; Sheardown, H. *Biomaterials* **2005**, *26*, 2391−2399.

(33) Xia, L. G.; Zhang, Z. Y.; Chen, L.; Zhang, W. J.; Zeng, D. L.; Zhang, X. L.; Chang, J.; Jiang, X. Q. *Eur. Cells Mater.* **2011**, *22*, 68−83.

(34) Li, L.; Mao, C. Y.; Wang, J. M.; Xu, X. R.; Pan, H. H.; Deng, Y.; Gu, X. H.; Tang, R. K. *Adv. Mater.* **2011**, *23*, 4695−4701.

(35) Liu, X. G.; Lin, K. L.; Wu, C. T.; Wang, Y. Y.; Zou, Z. Y.; Chang, J. *Small*, DOI: 10.1002/smll.201301633.

(36) Sing, K. S. W.; Everett, D. H.; Haul, R. A. W.; Moscou, L.; Pierotti, R. A.; Rouquerol, J.; Siemieniewska, T. *Pure Appl. Chem.* **1982**, *54*, 2201−2218.

(37) Ranella, A.; Barberoglou, M.; Bakogianni, S.; Fotakis, C.; Stratakis, E. *Acta Biomater.* **2010**, *6*, 2711−2720.

(38) Bucaro, M. A.; Vasquez, Y.; Hatton, B. D.; Aizenberg, J. *ACS Nano* **2012**, *6*, 6222−6230.

(39) Seo, C. H.; Furukawa, K.; Montagne, K.; Jeong, H.; Ushida, T. *Biomaterials* **2011**, *32*, 9568−9575.

(40) Posner, A. S.; Betts, F. *Acc. Chem. Res.* **1975**, *8*, 273−281.

(41) Kawasaki, T. *J. Chromatogr.* **1991**, *544*, 147−184.

(42) Onuma, K.; Ito, A. *Chem. Mater.* **1998**, *10*, 3346−3351.

(43) Kanzaki, N.; Onuma, K.; Ito, A.; Teraoka, K.; Tateishi, T.; Tsutsumi, S. *J. Phys. Chem. B* **1998**, *102*, 6471−6476.

(44) Kilpadi, K. L.; Chang, P. L.; Bellis, S. L. *J. Biomed. Mater. Res.* **2001**, *57*, 258−267.

(45) Stamm, C.; Sarret, Y.; Schmitt, D.; Thivoletet, J. *Pathol. Biol.* **1992**, *40*, 649−654.

(46) Preissner, K. T. *Annu. Rev. Cell Biol.* **2003**, *7*, 275−310.

(47) Cowles, E. A.; DeRome, M. E.; Pastizzo, G.; Brailey, L. L.; Gronowicz, G. A. *Calcif. Tissue Int.* **1998**, *62*, 74−82.

(48) Weiss, R. E.; Reddi, A. H. *Exp. Cell. Res.* **1981**, *133*, 247−254.

(49) Choi, Y. J.; Lee, J. Y.; Lee, S. J.; Chung, C. P.; Park, Y. J. *Biochem. Biophys. Res. Commun.* **2012**, *419*, 326−332.

(50) Lee, N. K.; Sowa, H.; Hinoi, E.; Ferron, M.; Ahn, J. D.; Confavreux, C.; Dacquin, R.; Mee, P. J.; McKee, M. D.; Jung, D. Y. *Cell* **2007**, *130*, 456−69.

(51) Tana, J.; Saltzman, W. M. *Biomaterials* **2004**, *25*, 3593−3601.